



OPEN

# Twinning in MAPbI<sub>3</sub> at room temperature uncovered through Laue neutron diffraction

Joachim Breternitz<sup>1</sup>✉, Michael Tovar<sup>1</sup> & Susan Schorr<sup>1,2</sup>

The crystal structure of MAPbI<sub>3</sub>, the signature compound of the hybrid halide perovskites, at room temperature has been a reason for debate and confusion in the past. Part of this confusion may be due to twinning as the material bears a phase transition just above room temperature, which follows a direct group–subgroup relationship and is prone to twinning. Using neutron Laue diffraction, we illustrate the nature of twinning in the room temperature structure of MAPbI<sub>3</sub> and explain its origins from a group-theoretical point-of-view.

Hybrid halide perovskites have caused a *nouvelle vague* in the research of photovoltaic absorber materials<sup>1,2</sup>. Within 10 years of their first consideration as solar absorbers, perovskite solar cells have reached over 25% efficiency<sup>3</sup>, close to the theoretical limit of such devices. While the rise in efficiency has provoked a huge interest in applied research—with some 4000 papers published on halide perovskites in 2019<sup>4</sup>, the efforts in structural elucidation have not always been commensurate. The crystal structure of methylammonium lead iodide (MAPbI<sub>3</sub>), for instance, has been a matter of debate and several, partially contradicting studies since its introduction into solar cells, although MAPbI<sub>3</sub> clearly is the signature compound of this family of materials<sup>5–11</sup>. One striking discrepancy in the structural characterisation of MAPbI<sub>3</sub> is the question as to whether it is ferroelectric at room temperature or not<sup>12–20</sup>. The generally accepted space group of MAPbI<sub>3</sub> at room temperature is *I4/mcm*<sup>5,7,9,11</sup>, a centrosymmetric space group that would not allow bulk ferroelectricity or further non-linear effects. However, there are striking reports of such behaviour<sup>16</sup> and we have recently discussed a deviation from the centrosymmetric crystal structure to a polar one (in space group *I4cm*) through the influence of the molecular cation on its surrounding iodide anions<sup>21</sup>.

One important factor in the structural elucidation of hybrid halide perovskites in general<sup>20,22</sup> and MAPbI<sub>3</sub> in particular<sup>23–26</sup> is their tendency for twinning. Commonly, this twinning can be associated with the phase transition from the high-temperature phase in the cubic aristotype to the lower temperature hettotypes. Ferroelectric compounds, for instance, do normally show heavy domain twinning, as this allows the compensation of the internal electric field through the formation of oppositely polarised domains. In the case of MAPbI<sub>3</sub> at room temperature, this would correspond to inversion twins in this case, as the inversion symmetry is lost between *I4/mcm* and *I4cm*. However, the observed domain structure of MAPbI<sub>3</sub> exhibits further twin laws, so that twinning solely due to the loss of inversion symmetry would not explain this fully. To account for this further twinning, namely ferroelastic twinning was proposed as primary driver<sup>23–26</sup>. Nonetheless, it should be emphasised that ferroelasticity and ferroelectricity are not mutually exclusive but can exist in the same phase, as for instance in BiFeO<sub>3</sub><sup>27</sup>.

At higher temperatures, MAPbI<sub>3</sub> crystallises in the cubic perovskite aristotype (space group *Pm $\bar{3}$ m*). When cooling below 330 K, the crystal structure changes into a tetragonal hettotype in *I4cm* or *I4/mcm*, where the latter is the centrosymmetric and the former the polar space group choice. Since the question of centrosymmetry is not touched in this work, we give both options in the further discussion. It needs to be mentioned that the structural differences are small, which makes the distinction between the choices even more subtle. Finally, at 160 K, the crystal structure of MAPbI<sub>3</sub> transitions into an orthorhombic perovskite subgroup (space group *Pnma*)<sup>11,28</sup>. The high temperature phase transition is reasonably close to room temperature, and, consequently, below the typical synthesis temperature in conventional solution based processes<sup>29</sup> as well as in other important techniques, such as the inverse temperature gradient method<sup>30</sup>. Therefore, MAPbI<sub>3</sub> necessarily undergoes a phase transition when synthesised through such a way. Herein, we studied a crystal that was synthesised at room

<sup>1</sup>Department Structure and Dynamics of Energy Materials, Helmholtz-Zentrum Berlin für Materialien und Energie GmbH, Hahn-Meitner-Platz 1, 14109 Berlin, Germany. <sup>2</sup>Department Geosciences, Freie Universität Berlin, Malteserstr. 74-100, 12249 Berlin, Germany. ✉email: Joachim.breternitz@helmholtz-berlin.de

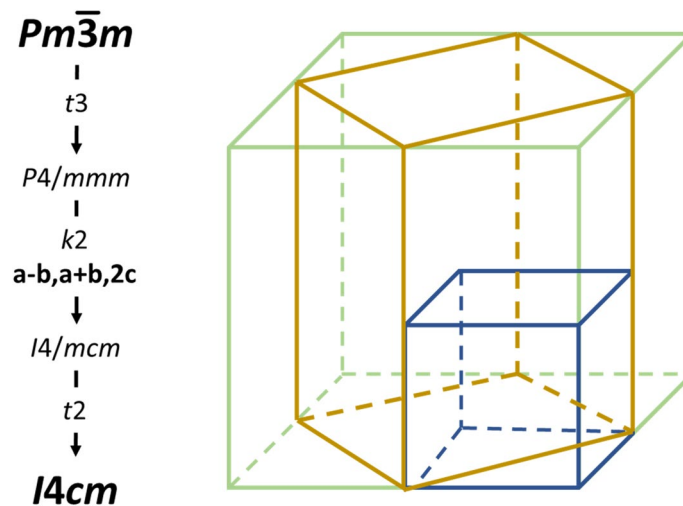


**Figure 1.** Group–subgroup relationship (left) between the cubic aristotype and the tetragonal hettotype in  $I4cm$  as the lowest possible space group type. Relationship between the unit cells of the cubic aristotype (blue), the standard setting of the tetragonal phase (gold) in  $I4cm$  ( $I4/mcm$ ) and the non-standard setting  $F4mc$  ( $F4/mmc$ ).

temperature and that was never heated above the cubic-tetragonal phase transition temperature. This study is seconded by an in-depth explanation of twinning in  $MAPbI_3$  in order to make the thematic approachable for the wider scientific community.

**Twinning in  $MAPbI_3$  through the cubic-to-tetragonal phase transition.** In a nutshell, twinned crystals are not composed of one single orientation, but are built up from different individual or domains. These domains or individual are, however, not randomly oriented but related through point symmetry elements, which must not be element of the space group symmetry, and can be categorised through the twinning element in inversion twins (related through inversion at a twin inversion centre), rotation twins (related through rotation at a twin axis) or reflection twins (related through reflection at a twin plane)<sup>31</sup>. For twinning that occurs during a phase transition, the twinning element needs to be a symmetry element of the high-symmetry structure, which is lost during the phase transition. Therefore, it is crucial to understand the group-subgroup relationships through the cubic-to-tetragonal phase transition in  $MAPbI_3$ . Prior work on twinning in the perovskite  $BaTiO_3$  may be taken as a first guidance<sup>32</sup>.

The phase transition from the cubic perovskite aristotype in  $Pm\bar{3}m$  to the room temperature perovskite structure in  $I4cm$  ( $I4/mcm$ ) follows a direct group-subgroup relationship and hence makes a second order phase transition possible. Even more importantly, the  $t3$  translationengleiche symmetry descent from  $Pm\bar{3}m$  to  $P4/mmm$  (Fig. 1) gives rise to the formation of triple twinning along the lost symmetry elements, i.e. the four threefold rotation axes. It is probably more illustrative to approach this from the unit cell dimensions (which are, of course, a consequence of the symmetry operations): while all three unit-cell axes are constrained to be equal in the cubic crystal system, only  $a$  and  $b$  have to fulfil this constraint in the tetragonal crystal system with  $c$  being independent of the other two. When transitioning from cubic to tetragonal, the choice of which of the three cubic unit-cell axes becomes the independent  $c$ -axis is arbitrary and hence three equivalent possibilities exist, standing perpendicular to each other.

A complication of the cubic-to-tetragonal transition in  $MAPbI_3$  is the symmetry descent from  $P4/mmm$  into the body-centred *klassengleiche* subgroup  $I4cm$  ( $I4/mcm$ ; Fig. 1). This transition is accompanied with a  $45^\circ$  rotation of the unit cell in the  $ab$ -plane and thus a change of the lattice constants in the manner  $a_{t-F} = \sqrt{2} \cdot a_c$  and  $c_{t-F} = 2 \cdot c_c$  (where the index  $t-F$  signifies the tetragonal body centred structure and  $c$  the cubic one). This has as consequence that direction and plane denominations change in a rather complex manner when transforming from  $Pm\bar{3}m$  to  $I4cm$  ( $I4/mcm$ ). Therefore, we chose a non-standard setting of the tetragonal unit cell in  $F4mc$  ( $F4/mmc$ ), where  $a_{t-F} = 2 \cdot a_c$  and  $c_{t-F} = 2 \cdot c_c$  (with  $t-F$  standing for tetragonal face centred; Fig. 1). Although this setting violates the Bravais rules of choosing the smallest possible unit cell, it has as major advantage that the directions correspond to each other in the tetragonal and the cubic lattices. Where appropriate, we will give directions and lattice planes for both settings. At room temperature, the lattice constants  $a$  and  $c$  with regard to the non-standard setting  $F4mc$  ( $F4/mmc$ ) are not greatly different ( $a_{t-F} = 12.507 \text{ \AA}$ ,  $c_{t-F} = 12.622 \text{ \AA}$ )<sup>21</sup>, which means that the diffraction spots of the different domains are close to each other to the extent that they nearly overlap completely—similar to a pseudo-merohedral twinning.

The twinning element in the cubic-to-tetragonal descent can, essentially, be any symmetry element lost during the phase transition. Most prominently, the aforementioned three-fold axes, which are defining the cubic crystal system, can become the twinning element. However, rotation twinning through  $90^\circ$  rotations along the  $\langle 100 \rangle_c$  axes or  $180^\circ$  rotation along the  $\langle 101 \rangle_c$  axes (Fig. 2) are also possible as well as reflection twinning on the  $\{011\}_c$ -planes<sup>23–25</sup>. These twin laws correspond to the respective four-fold and two-fold rotation symmetries that are lost when  $c$  becomes unequal from  $a$  and  $b$  in the transition from the cubic aristotype to the tetragonal

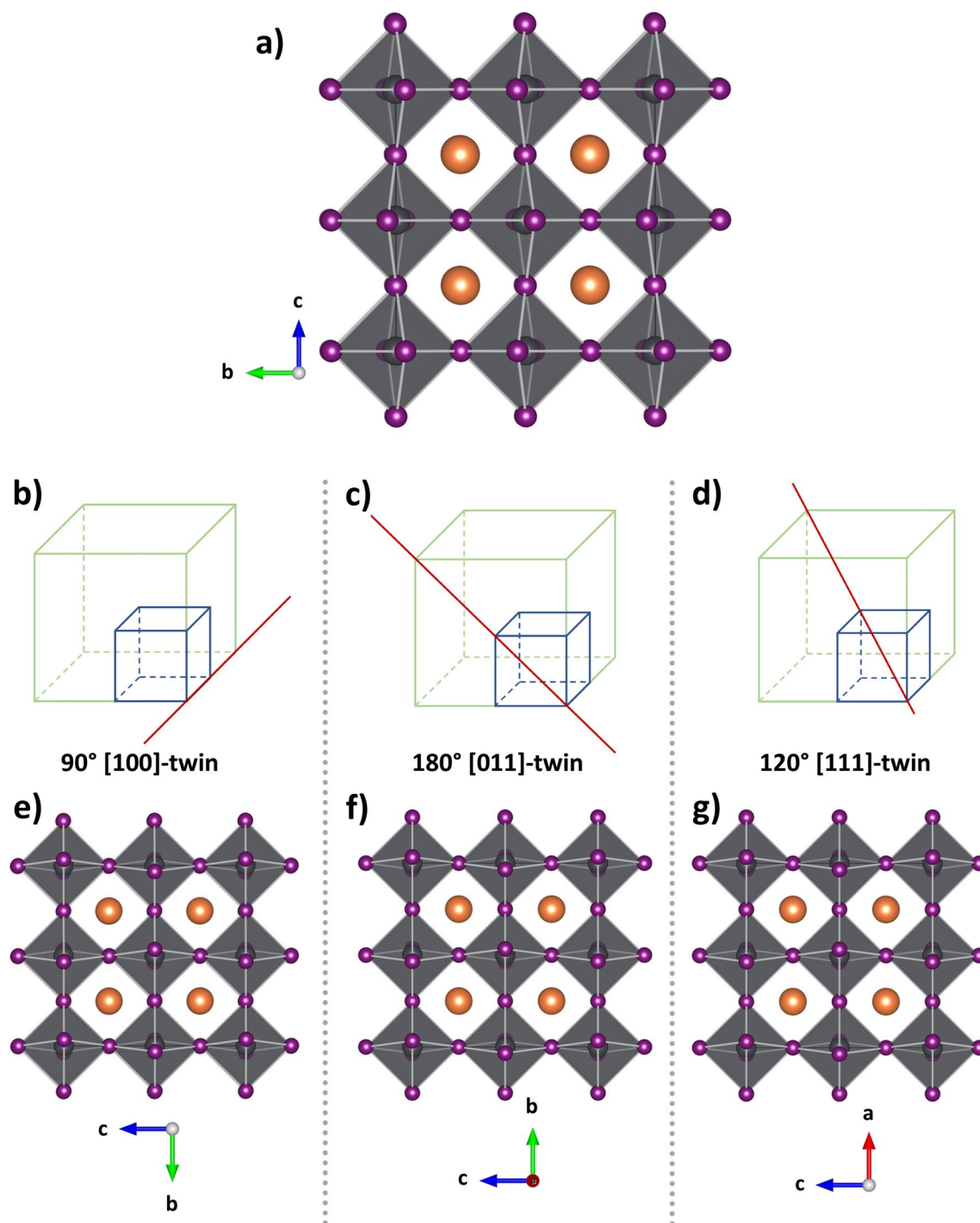


**Figure 2.** View of the crystal structure of MAPbI<sub>3</sub> along the *a*-axis (with crystallographic axes according to the non-standard setting  $F4mc$  ( $F4/mmc$ )) (a). Representations of different rotation twin axes (red lines) in the cubic (blue) and non-standard tetragonal (green) unit cells (b–d), and the resulting crystal structures with the twinning elements acting upon the original crystal structure (e–g). The molecular cation is simplified as orange spheres for the sake of visibility.

structure. However, these different twin laws are only seemingly contradictory, as they all represent the same phenomenon of axis permutations, i.e. of mapping the unique *c* axis on either *a* or *b* axis (Fig. 2). The difference between the different twin laws is the relative orientation of the *a* and *b* axes, which are symmetry equivalent in the tetragonal crystal system and are linked through four-fold rotation along the [001] axis and {100} mirror planes. Furthermore, a non-centrosymmetric space group would only be visible in the reflection intensities, not in their positions. A 120° rotation around one of the  $\langle 111 \rangle_c$  directions would hence produce twins that look identical to 90° twins around the  $\langle 100 \rangle_c$  directions or 180° twins around the  $\langle 101 \rangle_c$  directions. The same also

applies to the  $\{011\}_c$  reflection twins, that have been reported for this system. Finally, it needs to be noted that the presence of these twin laws does not rule the possibility of further inversion twinning out and, therefore, does not allow a conclusion on the absence of ferroelectricity: Inversion twinning would only be discernible under very specific measurement conditions, for instance at the proximity of an element's absorption edge, since Friedel's law is not strictly valid for these cases.

Two structural effects occur during the cubic-to-tetragonal phase transition within the crystal structure of  $\text{MAPbI}_3$ : (1) the molecular cations are no longer completely disordered, but orient along a number of preferred orientations and (2) a tilting of the  $[\text{PbI}_6]$  octahedra, both of which phenomena are probably interlinked. (1) The molecular cation in the cubic crystal structure is completely disordered and rotates freely in its cuboctahedral void<sup>33</sup>. In the room temperature crystal structure, though, it is still dynamically and statistically disordered but resides in well-defined preferential orientations in correspondence to its surrounding anions<sup>9</sup>. (2) The network of corner-sharing octahedra is undistorted in the cubic aristotype, i.e. all Pb–I–Pb angles are at  $180^\circ$  as dictated by the cubic symmetry. At room temperature, however, the octahedra are still untilted in one direction, i.e. the Pb–I–Pb angles along the crystallographic *c*-axis remain at  $180^\circ$ , but they are tilted within the *ab*-plane. From a crystallographic point of view, the  $[\text{PbI}_6]$  units no longer form exact octahedra in the tetragonal symmetry, but rather a square-planar bipyramid. The tilting of the inorganic  $[\text{PbI}_6]$  octahedra affects the size of the A-cation void (the place of the molecular  $\text{MA}^+$  cation) and on the electronic structure of the compound, which is mainly determined by the inorganic  $[\text{PbI}_6]$  octahedra network.

**Neutron Laue diffraction on  $\text{MAPbI}_3$ .** When applying diffraction methods, one is faced with two distinct problems: on the one hand powder diffraction techniques do not allow to distinguish between  $I4/mcm$  and  $I4cm$  as both belong to the same diffraction group<sup>34</sup>, i.e. they bear exactly the same translation symmetry and hence have the exact same systematic extinctions. Therefore, the only reflections that could differ overlap entirely. Single crystal studies, on the other hand, are flawed by heavy twinning of the crystals under consideration<sup>35</sup>, which is a consequence of the phase behaviour of this compound:  $\text{MAPbI}_3$  shows several structural phase transitions as outlined above.

Applying neutron Laue diffraction to study twinning in methylammonium lead iodide has two major advantages: first, neutrons interact much less strongly with matter than X-rays as neutrons are scattered on the atomic nuclei only, while X-rays are scattered on the electron shell. This implies that larger samples are necessary for neutron diffraction, but also less absorption for the electron rich atoms, such as lead and iodine. The larger size of the samples in neutron diffraction is indeed an advantage for this study, as these crystals typically exhibit more pronounced twinning. Furthermore, the architecture of the instrument is adapted to the use of larger crystals, which is not typically the case for X-ray diffraction with normally much smaller beam sizes of  $\approx 500 \mu\text{m}$ . The chosen setup allowed us to measure crystals of several millimetres size. Furthermore, Laue diffraction has a unique property: by using a polychromatic (“pink”) beam, each individual wavelength constructs its own Ewald sphere and, therefore, allows measurements with static detectors. In a typical single wavelength experiment—which is the standard in X-ray diffraction—the reflections move in and out of the detector plane (i.e. the plane in which the detector records) when the lattice constants change, for instance due to temperature. Therefore, it is generally necessary to measure a crystal during a rotation. In Laue diffraction, on the other hand, the polychromatic light produces reflection spots regardless of lattice parameter changes, and a crystal rotation is not necessary. Using powder diffraction does not allow the distinction of individual domains, since the three-dimensional information of the reflection position is merged into a single dimension, the scattering angle. However, the twinned reflections appear, because more than one domain overlay in a very specific way that is only discernible in three dimensions.

Due to the heavy twinning of these crystals, it was impossible to index the neutron Laue patterns using the unit cell parameters of the tetragonal room temperature crystal structure in the space group  $I4cm$  ( $I4/mcm$ ) directly. However, indexation was successful on basis of the cubic aristotype, as the differences in the reflection positions between the cubic aristotype and the tetragonal room-temperature structure are rather small. The *hkl* indices of the cubic indexing are given in Fig. 3, and can be linked to the tetragonal ones through the group-subgroup relationship between the two space groups (comp. Fig. 1). To distinguish the *hkl* indices in this work, tetragonal body centred, tetragonal face centred and cubic *hkls* indices are marked with an index *t*–I, *t*–F or *c*, respectively. Furthermore, we checked the successful indexation using the tetragonal subgroup  $P4/mmm$  (see “SI”), which is an intermediate space group in the symmetry descent but still bears approximately the same lattice constants as the cubic aristotype. In essence all three axis permutations appear as equally acceptable solutions for the indexation.

Using a static crystal in a special sample environment, we conducted temperature-dependent measurements using a specific crystal orientation. Due to the sample environment, we were limited in the choice of orientation, which is why the orientations at room temperature and at controlled temperature differ. The Laue patterns clearly show a twinning at room temperature in a pseudo-merohedral way: the double-maxima of the spots under consideration lie very close to each other (Fig. 4a). However, the Laue spots are clearly split at 300 K (Fig. 4b,c). On heating towards the tetragonal-to-cubic phase transition temperature at 330 K, the spots merge more and more into one single spot as the reflections of the twins become equivalent and hence the twinning domains are being merged during this process. The smooth merging of the domains can be taken as an indicator for the fact that this phase transition is actually an order–disorder phase transition.

In order to prove the nature of the twinning at room temperature, we recorded a series of diffraction images while turning the crystal in increments of  $1^\circ$  around the  $\omega$ -axis (i.e. the axis, on which the crystal is mounted and that is perpendicular to the beam path) without the heating equipment. What is observed in such an experiment is the movement of the diffraction spots through the detector plane, caused by diffraction at the same lattice plane from different wavelengths at different crystal rotations. According to Bragg's law, the separation of reflections





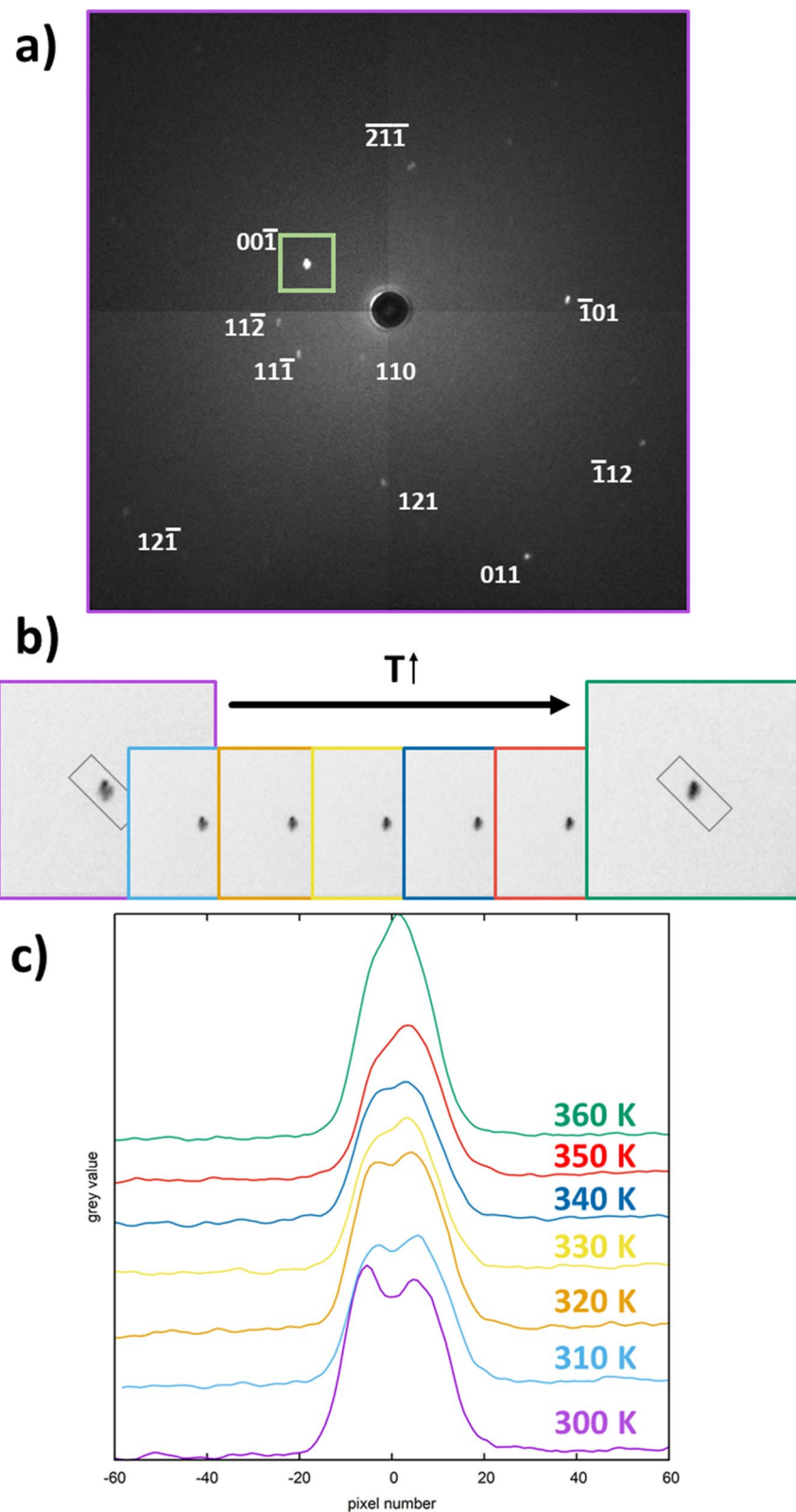


**Figure 4.** Indexation of the transmission Laue image of MAPbI<sub>3</sub> at 300 K in the cubic aristotype (a). The colormap was modified to increase spot visibility. The unaltered Laue image may be found as supplementary information. The inverted image of the area selected around the  $00\bar{1}_c$  reflection (grey frame in a) is shown at variable temperature (b). Rectangular profile integration at different temperatures (c) was performed for the selected area shown in b).

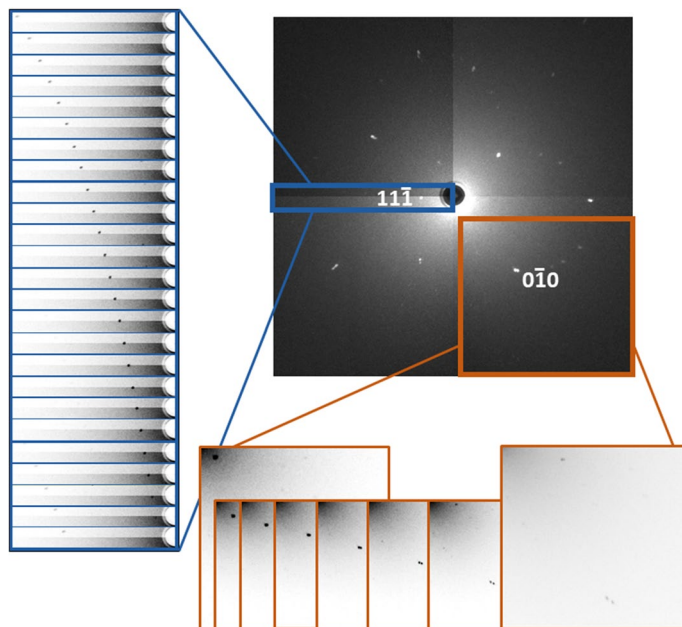


**Figure 5.** Changes of the  $0\bar{1}0_c$  spots during an  $\omega$ -scan ( $5^\circ$  steps) and of the  $11\bar{1}_c$  spots during the same scan ( $1^\circ$  steps). The cut-outs were inverted and brightness/contrast adjusted to increase visibility of the spots.

still bears approximately the same unit cell dimensions of the cubic space group (see “SI”), but clearly shows the twinning through axis permutation.

Received: 27 April 2020; Accepted: 15 September 2020

Published online: 06 October 2020

## References

- Igbari, F., Wang, Z.-K. & Liao, L.-S. Progress of lead-free halide double perovskites. *Adv. Energy Mater.* **9**, 1803150 (2019).
- Correa-Baena, J.-P. *et al.* The rapid evolution of highly efficient perovskite solar cells. *Energy Environ. Sci.* **10**, 710–727 (2017).
- <https://www.nrel.gov/pv/cell-efficiency.html>. Accessed 21 February 2020.
- Web of Science search for “perovskite solar cell” in 2019 yielded 3.853 hits. <https://apps.webofknowledge.com>. Accessed 21 February 2020.
- Poglitsch, A. & Weber, D. Dynamic disorder in methylammoniumtrihalogenoplumbates (II) observed by millimeter-wave spectroscopy. *J. Chem. Phys.* **87**, 6373–6378 (1987).
- Stoumpos, C. C., Malliakas, C. D. & Kanatzidis, M. G. Semiconducting tin and lead iodide perovskites with organic cations: Phase transitions, high mobilities, and near-infrared photoluminescent properties. *Inorg. Chem.* **52**, 9019–9038 (2013).
- Weller, M. T., Weber, O. J., Henry, P. F., Pumpo, A. M. D. & Hansen, T. C. Complete structure and cation orientation in the perovskite photovoltaic methylammonium lead iodide between 100 and 352 K. *Chem. Commun.* **51**, 4180–4183 (2015).
- Dong, Q. *et al.* Electron-hole diffusion lengths  $> 175 \mu\text{m}$  in solution-grown  $\text{CH}_3\text{NH}_3\text{PbI}_3$  single crystals. *Science* **347**, 967–970 (2015).
- Franz, A., Többsen, D. M. & Schorr, S. Interaction between cation orientation, octahedra tilting and hydrogen bonding in methylammonium lead triiodide. *Cryst. Res. Technol.* **51**, 534–540 (2016).
- Arakcheeva, A., Chernyshov, D., Spina, M., Forró, L. & Horvath, E.  $\text{CH}_3\text{NH}_3\text{PbI}_3$ : Precise structural consequences of water absorption at ambient conditions. *Acta Crystallogr. B* **72**, 716–722 (2016).
- Whitfield, P. S. *et al.* Structures, phase transitions and tricritical behavior of the hybrid perovskite methyl ammonium lead iodide. *Sci. Rep.* <https://doi.org/10.1038/srep35685> (2016).
- Kutes, Y. *et al.* Direct observation of ferroelectric domains in solution-processed  $\text{CH}_3\text{NH}_3\text{PbI}_3$  perovskite thin films. *J. Phys. Chem. Lett.* **5**, 3335–3339 (2014).
- Fan, Z. *et al.* Ferroelectricity of  $\text{CH}_3\text{NH}_3\text{PbI}_3$  perovskite. *J. Phys. Chem. Lett.* **6**, 1155–1161 (2015).
- Liu, S., Zheng, F., Grinberg, I. & Rappe, A. M. Photoferroelectric and photopiezoelectric properties of organometal halide perovskites. *J. Phys. Chem. Lett.* **7**, 1460–1465 (2016).
- Röhm, H., Leonhard, T., Hoffmann, M. J. & Colsmann, A. Ferroelectric domains in methylammonium lead iodide perovskite thin-films. *Energy Environ. Sci.* **10**, 950–955 (2017).
- Rakita, Y. *et al.* Tetragonal  $\text{CH}_3\text{NH}_3\text{PbI}_3$  is ferroelectric. *Proc. Nat. Acad. Sci.* **114**, E5504–E5512 (2017).
- Vorpahl, S. M. *et al.* Orientation of ferroelectric domains and disappearance upon heating methylammonium lead triiodide perovskite from tetragonal to cubic phase. *ACS Appl. Energy Mater.* **1**, 1534–1539 (2018).
- Wilson, J. N., Frost, J. M., Wallace, S. K. & Walsh, A. Dielectric and ferroic properties of metal halide perovskites. *APL Mater.* **7**, 10901 (2019).
- Röhm, H. *et al.* Ferroelectric properties of perovskite thin films and their implications for solar energy conversion. *Adv. Mater.* **31**, 1806661 (2019).
- Liu, W. *et al.* Twin domains in organometallic halide perovskite thin-films. *Crystals* **8**, 216 (2018).
- Breternitz, J., Lehmann, F., Barnett, S. A., Nowell, H. & Schorr, S. Role of the iodide–methylammonium interaction in the ferroelectricity of  $\text{CH}_3\text{NH}_3\text{PbI}_3$ . *Angew. Chem. Int. Ed.* **59**, 424–428 (2020).

22. Pham, H. T., Duong, T., Weber, K. J. & Wong-Leung, J. Insights into twinning formation in cubic and tetragonal multi-cation mixed-halide perovskite. *ACS Mater. Lett.* **2**, 415–424 (2020).
23. Hermes, I. M. *et al.* Ferroelastic fingerprints in methylammonium lead iodide perovskite. *J. Phys. Chem. C* **120**, 5724–5731 (2016).
24. Ren, Y., Oswald, I. W. H., Wang, X., McCandless, G. T. & Chan, J. Y. Orientation of organic cations in hybrid inorganic-organic Perovskite  $\text{CH}_3\text{NH}_3\text{PbI}_3$  from subatomic resolution single crystal neutron diffraction structural studies. *Cryst. Growth Des.* **16**, 2945–2951 (2016).
25. Rothmann, M. U. *et al.* Direct observation of intrinsic twin domains in tetragonal  $\text{CH}_3\text{NH}_3\text{PbI}_3$ . *Nat. Commun.* <https://doi.org/10.1038/ncomms14547> (2017).
26. Warwick, A. R., Íñiguez, J., Haynes, P. D. & Bristowe, N. C. First-principles study of ferroelastic twins in halide perovskites. *J. Phys. Chem. Lett.* **10**, 1416–1421 (2019).
27. Kubel, F. & Schmid, H. Growth, twinning and etch figures of ferroelectric/ferroelastic dendritic  $\text{BiFeO}_3$  single domain crystals. *J. Cryst. Growth* **129**, 515–524 (1993).
28. Lehmann, F. *et al.* The phase diagram of a mixed halide (Br, I) hybrid perovskite obtained by synchrotron X-ray diffraction. *RSC Adv.* **9**, 11151–11159 (2019).
29. Lehmann, F., Binet, S., Franz, A., Taubert, A. & Schorr, S. Cation and anion substitutions in hybrid perovskites: Solubility limits and phase stabilizing effects. in *2018 IEEE 7th World Conference on Photovoltaic Energy Conversion (WCPEC) (A Joint Conference of 45th IEEE PVSC, 28th PVSEC & 34th EU PVSEC)* (IEEE, 2018). <https://doi.org/10.1109/pvsc.2018.8547645>.
30. Saidaminov, M. I. *et al.* High-quality bulk hybrid perovskite single crystals within minutes by inverse temperature crystallization. *Nat. Commun.* <https://doi.org/10.1038/ncomms8586> (2015).
31. Hahn, T. & Klapper, H. “3.3 twinning of crystals” in *International Tables for Crystallography* Vol. D (ed. Authier, A.) 413–483 (Kluwer, 2013).
32. Cook, W. R. Domain twinning in barium titanate ceramics. *J. Am. Ceram. Soc.* **39**, 17–19 (1956).
33. Schuck, G., Lehmann, F., Ollivier, J., Mutka, H. & Schorr, S. Influence of chloride substitution on the rotational dynamics of methylammonium in  $\text{MAPbI}_{3-x}\text{Cl}_x$  perovskites. *J. Phys. Chem. C* **123**, 11436–11446 (2019).
34. Pecharsky, V. K. & Zavalij, P. Y. *Fundamentals of Powder Diffraction and Structural Characterization of Materials* 225 (Springer, Washington, 2009).
35. Szafranski, M. & Katrusiak, A. Mechanism of pressure-induced phase transitions, amorphization, and absorption-edge shift in photovoltaic methylammonium lead iodide. *J. Phys. Chem. Lett.* **7**, 3458–3466 (2016).
36. Tovar, M. *et al.* A Laue diffractometer for ambient and non-ambient neutron structural analysis. *Acta Crystallogr. A* **73**, C135 (2017).
37. Schumann, O. J. *Cologne Laue Indexation Program v4.0 RC1*, GNU General Public License, 2008. <http://clip4.sourceforge.net>.

### Author contributions

J.B. and S.S. conceived the original idea of the study. All authors developed the experimental strategy, J.B. and M.T. conducted the experiments. J.B. wrote the manuscript with input from all authors.

### Funding

Open Access funding enabled and organized by Projekt DEAL. This study was funded by Helmholtz-Zentrum Berlin für Materialien und Energie (Grant no. 17205680-EF).

### Competing interests

The authors declare no competing interests.

### Additional information

**Supplementary information** is available for this paper at <https://doi.org/10.1038/s41598-020-73487-1>.

**Correspondence** and requests for materials should be addressed to J.B.

**Reprints and permissions information** is available at [www.nature.com/reprints](http://www.nature.com/reprints).

**Publisher's note** Springer Nature remains neutral with regard to jurisdictional claims in published maps and institutional affiliations.



**Open Access** This article is licensed under a Creative Commons Attribution 4.0 International License, which permits use, sharing, adaptation, distribution and reproduction in any medium or format, as long as you give appropriate credit to the original author(s) and the source, provide a link to the Creative Commons licence, and indicate if changes were made. The images or other third party material in this article are included in the article's Creative Commons licence, unless indicated otherwise in a credit line to the material. If material is not included in the article's Creative Commons licence and your intended use is not permitted by statutory regulation or exceeds the permitted use, you will need to obtain permission directly from the copyright holder. To view a copy of this licence, visit <http://creativecommons.org/licenses/by/4.0/>.

© The Author(s) 2020